12th International Symposium on Turbulence and Shear Flow Phenomena (TSFP12)
Osaka, Japan (Online), July 19-22, 2022

SIMULTANEOUS VELOCITY AND TEMPERATURE MEASUREMENTS IN THE LAMINAR BOUNDARY LAYER OF A MELTING VERTICAL ICE FACE

Pamoda Herath
Department of Mechanical Engineering
The University of Melbourne
Victoria 3010 Australia
jherath@student.unimelb.edu.au

Saurabh Pathak
Department of Mechanical Engineering
The University of Melbourne
Victoria 3010 Australia
pathak@unimelb.edu.au

Bishakhdatta Gayen
Department of Mechanical Engineering
The University of Melbourne
Victoria 3010 Australia
CAOS
Indian Institute of Science
bishakhdatta.gayen@unimelb.edu.au

Joseph Klewicki
Department of Mechanical Engineering
The University of Melbourne
Victoria 3010 Australia
klewicki@unimelb.edu.au

Jimmy Philip
Department of Mechanical Engineering
The University of Melbourne
Victoria 3010 Australia
jimmyp@unimelb.edu.au

ABSTRACT

The present experimental investigation is motivated by an aim to understand the processes by which the Antarctic ice shelves melt, under convective flow conditions. The density driven boundary layer flow that forms next to a melting ice-water interface has a direct influence on the heat and salt transfer to the ice that further determines the ice ablation rate. High resolution velocity and temperature measurements in this boundary layer are thus useful to understand and estimate the melting process of a vertical ice face. As a starting point, in the present paper we consider a relatively small vertical ice block resulting in a laminar melt boundary layer, unlike the field situation where the boundary layer is turbulent. Single component molecular tagging velocimetry (1c-MTV) and Molecular tagging thermometry (MTT) are employed to simultaneously measure the boundary layer vertical flow velocity and temperature close to the phase-change ice-water interface in a laboratory setup for different ambient water temperatures and salinities. Also, the ice face ablation rate is estimated by determining the position of the ice water interface as a function of time. The experimental findings are compared with idealised direct numerical simulations (DNS) that solve the three-dimensional and non-hydrostatic Navier-Stokes equations under similar conditions as well as with the similarity solution for an isothermal wall.

Introduction

When an ice face is in contact with saline water, due to the density difference between cold fresh water released from the interface and ambient saline water, a buoyancy driven convective boundary layer flow forms next to the ice water interface. The nature of this boundary layer flow is determined by the temperature and salinity of the ambient water. Usually boundary layer flow starts as a laminar flow and becomes turbulent as it flows along the interface. The ice melting process is mainly driven by the heat and salt transport to the ice interface (Josberger & Martin, 1981; Kerr & McConnochie, 2015; Gayen *et al.*, 2016) across the boundary layer. Therefore, heat and salt conservation at the interface determine ice ablation rate. The heat flux balance at the interface is given by

$$Q^H_{ice} - Q^H_w = Q_m, \tag{1}$$

relating the heat flux in to the water (Q^H_w) and in the ice (Q^H_{ice}) to the latent heat of ice melting (Q_m), where $Q^H_w = \rho_w c_w \kappa_T \partial T/\partial x$ and $Q_m = \rho_i L V$. Here ρ_w, c_w and κ_T are the density, specific heat and thermal diffusivity of the water, whereas ρ_{ice}, L and V are the density, specific latent heat and ablation velocity of the ice, respectively. The direction perpendicular to the ice-face and into water is x (c.f., figure 1) and T is the temperature. The heat flux into the ice is negligible, $Q^H_{ice} \approx 0$ (Holland & Jenkins, 1999), and therefore the heat balance at the interface is given by

$$\rho_{ice} L V = -\rho_w c_w \kappa_T \frac{\partial T}{\partial x}. \tag{2}$$

Similarly, for salt the flux balance,

$$Q^S_{ice} - Q^S_w = Q_S, \tag{3}$$

where Q^S_w is the salt flux in to the water, Q^S_{ice} is the salt flux in the ice and Q_S is the brine rejection flux. Here Q^S_{ice} is negligible and the salt balance is then given by

$$\rho_{ice} S_i V = -\rho_w \kappa_S \frac{\partial S}{\partial x}, \tag{4}$$

where κ_S is the salt diffusivity in water, and this determines the salinity at the interface (S_i). S_i determines the interface temperature (T_i) according to freezing point depression equation of salt water,

$$T_i = mS_i, \tag{5}$$

where $m = -6\times10^{-2}{}^\circ C/‰$(Josberger & Martin, 1981).

Through various experimental and numerical studies (Josberger & Martin, 1981; Kerr & McConnochie, 2015; McConnochie & Kerr, 2016; Gayen *et al.*, 2016) it has been found that the nature of the boundary layer flow that forms next to phase changing interface directly affects the melt rate of the ice-face. In order to study the efficiency of the heat transport across the boundary layer, which is ultimately important to quantify the melt-rate of ice, studying the convective boundary layer flow is important. Full temperature and velocity profiles in the melt plume are only available through Direct Numerical Simulations (Gayen *et al.*, 2016; Mondal *et al.*, 2019), and to date no experimental methodology has been developed to obtain high resolution velocity and temperature measurements in this phase change boundary layer. The present study focuses on developing an experimental procedure to obtain simultaneous velocity and temperature measurements in a laminar boundary layer flow close to a vertically melting ice face. The longer term aim is to understand the Antarctic ice-shelf melting process and boundary layer dynamics that are associated with a turbulent boundary layer flow.

Single component molecular tagging velocimetry (1c-MTV) is employed to estimate the boundary layer vertical flow velocity close to the phase-change ice-water interface in a laboratory setup for different ambient water temperatures in fresh and saline environments. In the MTV technique, phosphorescent molecules excited by an ultra-violet laser are used as a Lagrangian tracer, and velocities are determined by two images separated by a specified delay time as acquired by a gated intensified camera (Hu & Koochesfahani, 2006; Agrawal *et al.*, 2021). Here we acquire velocity data within and outside of the melt plume. Simultaneous temperature measurements in the boundary layer are also carried out by molecular tagging thermometry (MTT). MTT leverages the fact that the decay rate of the phosphorescence is uniquely temperature dependent (Gendrich *et al.*, 1997). The standard MTT methodology is modified in the present case by employing different camera exposure times for the two required images. This enables larger inter-frame delays, which makes it possible to measure temperature and relatively small magnitudes of velocity simultaneously. In addition to flow measurements, the ice ablation velocity is also measured separately.

A direct numerical simulation (DNS) model (Gayen *et al.*, 2014) that solves the three-dimensional and non-hydrostatic Navier-Stokes equations, along with the incompressiblity condition and heat and salinity conservation equations is used to simulate the ice melting and boundary layer formation process in the water tank. The DNS model used either linear or non linear equations of state (EoS). The DNS results are herein compared to the experimentally measured data.

The Navier–Stokes, mass, heat and salt conservation equations that are used in the DNS model are

$$\nabla \cdot \tilde{u} = 0, \tag{6}$$

$$\frac{\partial \boldsymbol{u}}{\partial t} + (\boldsymbol{u}\cdot\nabla)\boldsymbol{u} = \frac{-\nabla p^*}{\rho_0} + \nu\nabla^2\boldsymbol{u} - \frac{\rho^*}{\rho_0}\tilde{g}, \tag{7}$$

$$\frac{\partial T^*}{\partial t} + (\boldsymbol{u}\cdot\nabla)T^* = \kappa_T\nabla^2 T^*, \tag{8}$$

$$\frac{\partial S^*}{\partial t} + (\boldsymbol{u}\cdot\nabla)S^* = \kappa_S\nabla^2 S^*. \tag{9}$$

Here ρ^*, T^* and S^* are changes in density, temperature and salinity. ρ_0 is reference density, ν is kinematic viscosity, $\boldsymbol{u} = (u, v, w)$, $\boldsymbol{g} = (0, 0, g)$ and p^* is the pressure deviation from its reference value.
The change in density (ρ^*) for linear EoS DNS is given by,

$$\rho^* = \rho_0(\beta S^* - \alpha T^*). \tag{10}$$

Here β is the haline contraction coefficient and α is the thermal expansion coefficient at the ambient water temperature and salinity. Depending on the ambient temperature and salinity β varies in the range of 7.6×10^{-4} to 8.2×10^{-4}kg/g while α ranged from 0 to $2.1\times10^{-4}{}^\circ C^{-1}$.
For non linear EoS DNS, change in density (ρ^*) is evaluated by,

$$\rho^* = \rho - \rho_0 \tag{11}$$

where $\rho = f(T, S)$ as given in TEOS10 (McDougall & Barker, 2011).

In this study the importance of using non-linear equation of state is investigated by comparing the experiments with DNS that used both linear and non-linear models.

Experiments

As shown in figure 1, Experiments were performed in a small water tank with 9 cm depth and a square base of 18 cm length and width. One sidewall of the tank has a fused silica window to allow UV laser beam access. At the beginning of

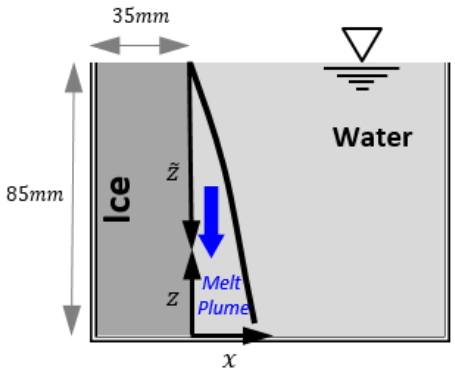

Figure 1. Schematic of water tank and ice block showing a downward flowing boundary layer flow.

the experiments, as show in figure 1, an ice block with 35 mm thickness was placed at one end of the tank. Once the ice face is in contact with the water, a buoyancy driven laminar boundary layer flow forms next to ice-water interface.

In this study, the experiments were conducted under different ambient water temperatures and salinities, and depending on the ambient conditions the flow can be upwards or downwards. Velocity and temperature profiles were obtained at $\tilde{z} = 58$mm ($\tilde{z}$ origin at top, c.f., figure 1) for downward flowing boundary layer cases whereas at $z = 58$mm (from bottom) for upward flowing boundary layer cases. The Grashof number along the z-direction defined as $Gr_z \equiv g(\Delta\rho)z^3/\nu^2\rho_0$. Here $\Delta\rho$ is the difference between water density at the interface and water density in the far field. At the given z location Gr_z varies in the range of 1×10^6- 1.2×10^7 depending on T_∞. Note that the critical Grashof number for transition from laminar to turbulent flow on a solid vertical wall varies from 10^9- 10^{10}.

The full MTV/MTT experimental setup mainly consist of the water tank, a pulsed UV laser, and an intensified gated camera that can capture 5 frames per second with an image resolution of 1024×1024 pixels. A digital delay generator is used to synchronize the camera and the laser. The laser beam is guided to the fused silica window using an optical arrangement consisting of UV mirrors. A pinhole arrangement is then used to obtain a thin laser line to excite phosphorescent molecules within the water. Images captured by the camera are logged using a host computer. The arrangement of the different components of the experimental setup is illustrated in figure 2. In these experiments the ice block is created in a mold using slightly heated water (to reduce bubble formation) and keeping it in a freezer typically for overnight. Once the ice is frozen a small layer of sufficiently diluted MTV solution is poured on the ice-face (where melting happens), and allowed to freeze again. This layer of ice with the phosphorescence molecules ensures that when the ice melts, the melt plume has sufficient MTV signal during the experiments.

In some cases, a separate set of experiments were carried out to measure the ice melting rate for each ambient water temperature. Here, however, the laser was not used. Rather, an intense white light source was used to illuminate the melting ice-face. The receding position of the ice-water interface was obtained as a function of time using image analysis, and from this the melt rate of ice (reduction of the ice thickness per unit time) was estimated..

The numerical setting of the DNS model is reported in Gayen *et al.* (2014). The computational domain is similar to the water tank. The length measured in the x direction is, however, infinite in the DNS domain. This serves to preserve mass conservation in the domain as the ice face melts, whereas in the experiments the melt water simply (depending on the ambient conditions) accumulates at the top or at the bottom of the tank, forming a mild recirculation over an extended period.

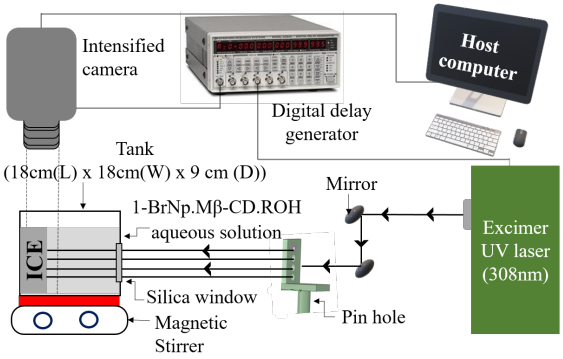

Figure 2. Schematic diagram of the experimental setup and the arrangement of its components.

Results

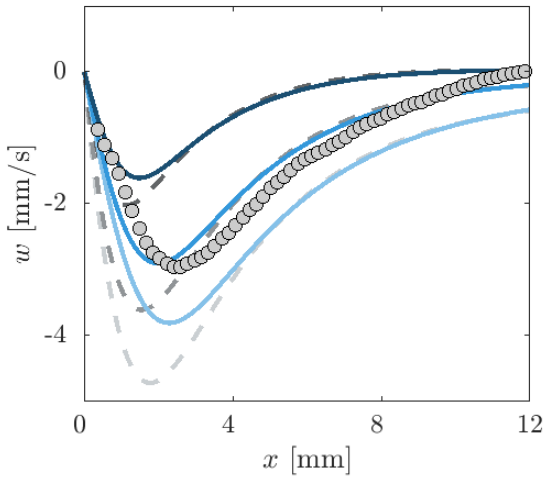

Figure 3. Comparison of experimental (symbols), DNS with linear equation of state (dashed lines) and DNS with non-linear equation of state (solid lines) velocity (w) profiles for $T_\infty = 10°C$ and $S_\infty = 0$. Experimental results are obtained at $\tilde{z} = 58$mm, i.e., $z = 27$mm. All DNS results are obtained at z values of 35, 55, and 75mm and the colour gets darker as z increases.

Averaged velocity and temperature profiles obtained experimentally for different ambient conditions are compared with direct numerical simulations (DNS). DNS uses either a linear or non-linear equation of state to relate temperature and salinity to density. Figure 3 shows a comparison between the experimental (in symbols) and DNS vertical velocity (w)

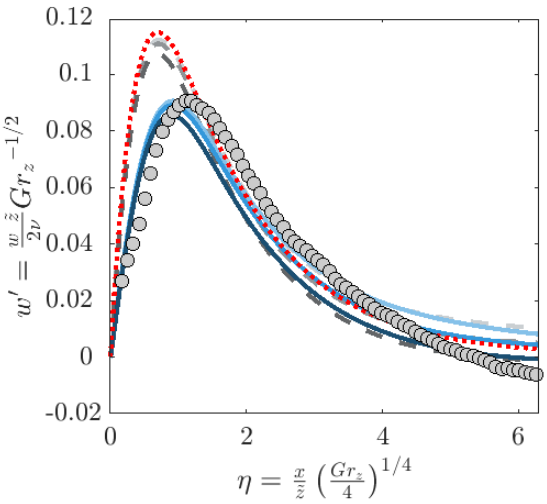

Figure 4. Comparison of non-dimensionalized experimental and DNS (linear and non-linear equation of state) Velocity (w^*) profiles with analytical solution of natural convection over isothermal flat plate for $Pr = 10$ (red dotted lines), for $T_\infty = 10°C$ and $S_\infty = 0$.

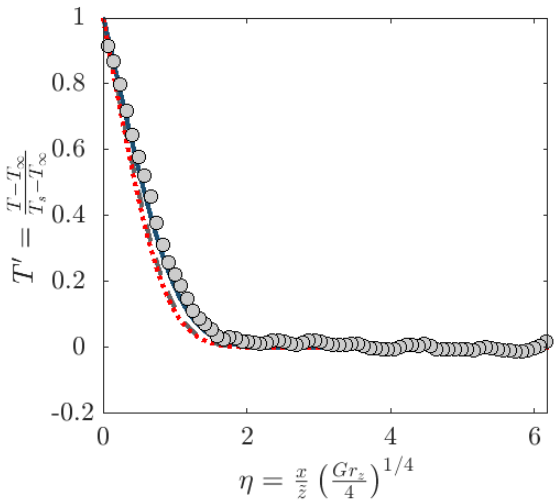

Figure 5. Comparison of non-dimensionalized experimental and DNS (linear and non-linear equation of state). Temperature (T^*) profiles with analytical solution of natural convection over isothermal flat plate for $Pr = 10$ (red dotted lines), for $T_\infty = 10°C$ and $S_\infty = 0$.

profiles obtained for ambient water conditions of $T_\infty = 10°C$ and $S_\infty = 0$ (ambient water salinity). Here the dashed lines are for the DNS using a linear equation of state (EoS), while non-linear EoS results are in solid lines. From the figure, it is apparent that the measured data are well within the range of velocities obtained from the DNS. We note that the precise velocity magnitudes are quite sensitive to the accurate choice of the z-location. It is well-known that the boundary layer does not start precisely at the 'leading-edge' or the free-surface, and a correction in terms of virtual origin is usually required.

Both the experimental and the DNS profiles obtained for fresh water ($S_\infty = 0$) are non-dimensionalized and compared with the analytical similarity solution for natural convection over an isothermally cooled vertical flat plate (Ostrach, 1952) at a fixed Prandtl number of 10 and a fixed thermal expansion coefficient (β) (i.e linear equation of state) as shown in figure 4. It can be observed that after a virtual origin shift of 28mm, non-dimensionalized experimental velocity profiles nearly coincide with the nonlinear EoS DNS profiles. From figure 3 and 4 it is evident that the peak velocity location and magnitude of the nonlinear EoS DNS velocity profiles are in better agreement with the measured profile than the linear EoS DNS results and similarity solution. This suggests the role of nonlinear EoS on momentum transport. These differences are, however, not apparent in the temperature boundary layer profiles (see figure 5). Here, careful inspection reveals that close to the ice surface (say at $\eta \approx 1$) the non-linear (solid lines), rather than linear (dashed-lines), compare more favorably with the experimental data. This further highlights the apparent importance of non-linear EoS in numerical simulations.

Figures 6 and 7 show velocity and temperature profiles from three different low ambient temperature cases; $T_\infty = 10°C$ and $S_\infty = 0$ (black), $T_\infty = 4°C$ and $S_\infty = 0$ (green) and $T_\infty = 4°C$ and $S_\infty = 35$ g/kg (purple). In the first(black) case the flow is downward because colder water near the melting ice face is denser than the warm ambient water. But the flow is upward in the second(green) case because fresh water density is maximum at $4°C$, and colder water near the melting ice face is less dense than the ambient water at $4°C$. The third(purple) case has a complex boundary layer flow that consists of a inner upward flow and outer downward flow that is driven by the combined effect of temperature and salinity on the water density. In all these cases, measurements have captured not only the flow directions but also the velocity magnitudes and peak locations with a good agreement with the DNS.

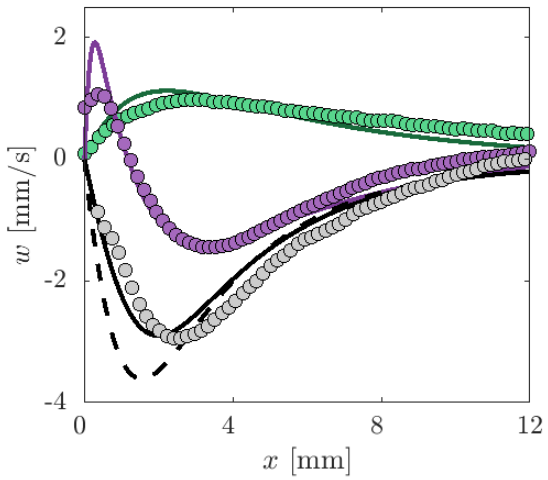

Figure 6. (a) Velocity (w) profiles for $T_\infty = 10°C$ and $S_\infty = 0$ (black), $T_\infty = 4°C$ and $S_\infty = 0$ (green) and $T_\infty = 4°C$ and $S_\infty = 35$ g/kg (purple) obtained at $\tilde{z} = 58$mm for downward flowing boundary layers and $z = 58$mm for upward flowing boundary layer flows. (symbols- experiments, solid lines-non linear DNS, dashed lines-linear DNS)

Figure 8 illustrates how ice melt-rates (estimated by locating the ice-water interface as a function of time) compare with the melt-rates obtained from DNS for 5 different am-

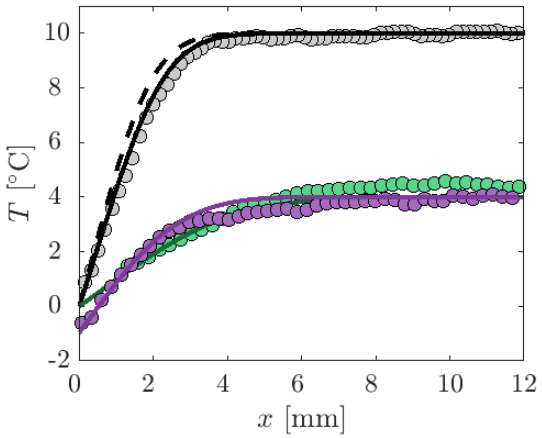

Figure 7. Temperature (T) profiles for $T_\infty = 10°C$ and $S_\infty = 0$ (black), $T_\infty = 4°C$ and $S_\infty = 0$ (green) and $T_\infty = 4°C$ and $S_\infty = 35$ g/kg (purple) obtained at $\tilde{z} = 58$mm for downward flowing boundary layers and $z = 58$mm for upward flowing boundary layer flows. (symbols- experiments, solid lines-non linear DNS, dashed lines-linear DNS)

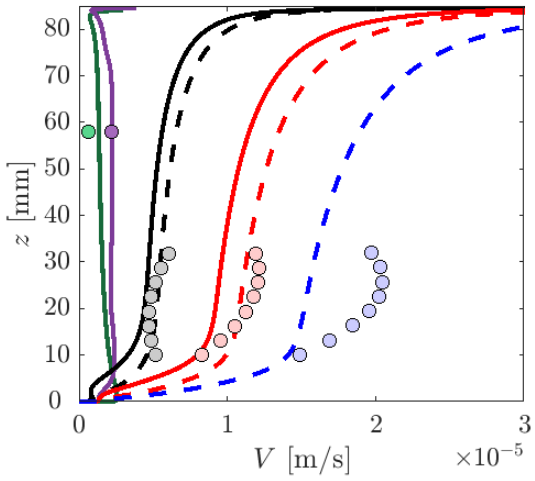

Figure 8. (c) Ice melt rate profiles for $T_\infty = 20°C$ and $S_\infty = 0$ (Blue), $T_\infty = 15°C$ and $S_\infty = 0$ (Red), $T_\infty = 10°C$ and $S_\infty = 0$ (Black), $T_\infty = 4°C$ and $S_\infty = 0$ (Green) and $T_\infty = 4°C$ and $S_\infty = 35$ g/kg (Purple). Here experimental results are in symbols, DNS with linear equation of state in dashed lines and DNS with non-linear equation of state in solid lines.

bient conditions. It is observed that the melt-rates increase with increasing ambient water temperature and salinity. For downward boundary layer flows the melt-rate increases with increasing z, whereas it decreases with increasing z for upward boundary layer flows. These trends can be explained using equation 8, where ablation velocity V is directly proportional to $\partial T/\partial x$ at the interface. Figure 7 reveals that the temperature gradient at the interface is much higher for the $T_\infty = 10°C$ case compared to the $T_\infty = 4°C$ cases due to a higher temperature difference between the interface and ambient water. Therefore, ice melting is higher in the $T_\infty = 10°C$ case compared to $T_\infty = 4°C$ cases. Furthermore, due to freezing point depression (described by the equation 5), as the water salinity increases, ice melts at temperatures below $0°C$. As a result, this increases the temperature difference between the interface and ambient water and consequently increases the temperature gradient at the interface. This is apparent when the $T_\infty = 4°C$ and $S_\infty = 0$ case is compared to the $T_\infty = 4°C$ and $S_\infty = 35$ g/kg case in figure 7. Therefore, for the $T_\infty = 4°C$ and $S_\infty = 35$ g/kg case the melt rate is higher compared to the $T_\infty = 4°C$ and $S_\infty = 0$ case in figure 8. Further, the thermal boundary layer thickness grows in the flow direction, decreasing $\partial T/\partial x$ in that direction. That is, although the thickness of the BL increases, the temperature difference remains constant, and thus the ice ablation velocity decreases in the flow direction.

From figure 8 it can be observed that both experiments and DNS results capture these trends while also showing reasonable agreement with each other.

Conclusion

A molecular tagging based simultaneous velocity and temperature measurement methodology was developed to experimentally measure the phase change boundary layer flow along a melting vertical ice face. Boundary layer velocity and temperature measurements show good agreement with DNS. It can be observed that experimental velocity and temperature measurements match better with the DNS that employed a nonlinear equation of state, as compared to a linear EoS or the solid wall similarity solution. The reason for this is ice melting process is driven by the nonlinear variation of water density within the boundary layer. Melt rates of the ice were quantified by tracking the interface, and these measurements also match reasonably well with the DNS meltrates. The effect of salinity of ambient water on boundary layer dynamics and ice melting process was also presented.

REFERENCES

Agrawal, Tanmay, Ramesh, Bhaarath, Zimmerman, Spencer J, Philip, Jimmy & Klewicki, Joseph C 2021 Probing the high mixing efficiency events in a lock-exchange flow through simultaneous velocity and temperature measurements. *Phys. Fluids* **33** (1), 016605.

Gayen, Bishakhdatta, Griffiths, RossW & Hughes, GrahamO 2014 Stability transitions and turbulence in horizontal convection. *J. Fluid Mech.* **751**, 698.

Gayen, Bishakhdatta, Griffiths, Ross W & Kerr, Ross C 2016 Simulation of convection at a vertical ice face dissolving into saline water. *J. Fluid Mech.* **798**, 284.

Gendrich, CP, Koochesfahani, MM & Nocera, DG 1997 Molecular tagging velocimetry and other novel applications of a new phosphorescent supramolecule. *Exp. Fluids* **23** (5), 361–372.

Holland, David M & Jenkins, Adrian 1999 Modeling thermodynamic ice–ocean interactions at the base of an ice shelf. *Journal of Physical Oceanography* **29** (8), 1787–1800.

Hu, Hui & Koochesfahani, Manoochehr M 2006 Molecular tagging velocimetry and thermometry and its application to the wake of a heated circular cylinder. *Meas Sci Technol.* **17** (6), 1269.

Josberger, Edward G & Martin, Seelye 1981 A laboratory and theoretical study of the boundary layer adjacent to a vertical melting ice wall in salt water. *J. Fluid Mech.* **111**, 439–473.

Kerr, Ross C & McConnochie, Craig D 2015 Dissolution of a vertical solid surface by turbulent compositional convection. *J. Fluid Mech.* **765**, 211.

McConnochie, Craig D & Kerr, Ross C 2016 The turbulent wall plume from a vertically distributed source of buoyancy. *J. Fluid Mech.* **787**, 237.

McDougall, Trevor J & Barker, Paul M 2011 Getting started with teos-10 and the gibbs seawater (gsw) oceanographic toolbox. *Scor/Iapso WG* **127**, 1–28.

Mondal, Mainak, Gayen, Bishakhdatta, Griffiths, Ross, Kerr, Ross *et al.* 2019 Ablation of sloping ice faces into polar seawater .

Ostrach, Simon 1952 An analysis of laminar free-convection flow and heat transfer about a flat plate parallel to the direction of the generating body force. *Tech. Rep.*. National Aeronautics and Space Administration Cleveland Oh Lewis Research Center.